Available online at www.sciencedirect.com
SCIENCE DIRECT®
International Journal of Mass Spectrometry 229 (2003) 67–76
International Journal of Mass Spectrometry
www.elsevier.com/locate/ijms

Laser-induced fluorescence/ion trap as a detector for mass spectrometric analysis of nanoparticles

W.-P. Peng [a,b], Y. Cai [a], Y.T. Lee [a,b], H.-C. Chang [a,*]

[a] *Institute of Atomic and Molecular Sciences, Academia Sinica, P.O. Box 23-166, Taipei 106, Taiwan*
[b] *Department of Physics, National Taiwan University, Taipei 106, Taiwan*

Received 23 December 2002; accepted 4 March 2003

Abstract

A novel detector is developed for ion trap mass spectrometry of nanoparticles. The detector, composed of a laser, a photomultiplier, and a quadrupole ion trap, is designed specifically for probing nanoparticles that are intrinsically fluorescent or extrinsically labeled with dye molecules. Using this detector, we have been able to obtain the mass spectra of fluorescein-labeled polystyrene spheres of 27 and 110 nm in diameter with a home-built quadrupole ion trap mass spectrometer operating in the mass-selective instability and frequency scan modes. It represents advancement in mass spectrometric analysis of nanoparticles with m/z (mass/charge) beyond 10^6. In this article we describe in detail the characterization of the laser-induced fluorescence/ion trap as a nanoparticle detector. Important parameters such as q_z and particle damping/dumping times are analyzed both experimentally and theoretically. The utility of this new ion detection method in mass spectrometric analysis of biological particles is discussed.

Keywords: Laser-induced fluorescence; QITMS; Nanoparticles

1. Introduction

The development of quadrupole ion trap mass spectrometers (QITMS) can be divided into three important ages: mass-selective detection, mass-selective storage, and mass-selective ejection [1]. Except that of Wuerker et al. [2], most of the developments have involved operation of the quadrupole ion traps in the low m/z (mass/charge) region. This is mainly due to limitations of the ion detection methods, which rely heavily on the use of electron multipliers and related devices as the detector [3]. Using microchannel plates (MCP) as an example, the detection efficiency of the plates decreases markedly with molecular mass from ∼80% of $m = 2$ kDa to ∼5% of $m = 10$ kDa at an ion impact energy of 10 keV [4]. An additional limitation of the contemporary QITMS is that the trap driving frequency is typically maintained in the range of 1 MHz, not optimized for the analysis of high-mass molecules and particles [5]. Schlunegger et al. [6] have recently adopted a different approach by using frequency scan at a constant voltage, instead of voltage scan at a constant frequency, with a wide band power amplifier. The authors managed to obtain the mass spectra of singly charged protein molecules (up to 150 kDa) in a quadrupole ion trap with the frequency swept from 20 to 10 kHz. Extending the study to higher-mass molecules ($m > 1$ MDa), however, was still hampered by the use of an electron multiplier, despite that the multiplier came with a conversion dynode floated at −25 kV to enhance the detection efficiency [7].

New methods have been developed to detect high-mass biomolecules as well as nanometer-sized particles [8–16]. The methods can principally be classified by two groups: inductive detectors [8–13] and cryogenic detectors [14–17]. The former involves detection of inductive currents of multiply charged particles as they pass through an image charge detection tube, while the latter involves measurement of energy deposition on a cold detector element from particle impacts. Both methods help to extend mass analysis ranges and improve ion detection limits of high-mass species. Benner [12] has shown that, by using the inductive detector, one can obtain the mass spectrum of 4.3-kb DNA in a gated electrostatic ion trap with a mass resolution of 25. The

* Corresponding author. Tel.: +886-2-23620200.
E-mail address: hcchang@po.iams.sinica.edu.tw (H.-C. Chang).

1387-3806/$ – see front matter © 2003 Elsevier B.V. All rights reserved.
doi:10.1016/S1387-3806(03)00257-4

measurement, however, requires the particles to carry more than 250 charges in order to be detected and thus use of electrospray ionization (ESI) as an ion source becomes a necessity. When matrix-assisted laser desorption/ionization (MALDI) is adopted as the ion source, Hilton et al. [15] suggested that the cryogenic detector would be a better diagnostic tool since it is sensitive to weakly ionizing and slowly moving molecules, in contrast to MCP whose detection efficiency falls rapidly with mass. Unfortunately, the application requires the detector to operate at very low temperatures (<2 K) and is disadvantageous in that the detector has a relatively long response time (∼1 μs) and a small detection area (<1 mm^2) [17].

Here we propose an alternative detection scheme to probe both high-mass biomolecules and nanometer-sized particles. The method is rooted on the pioneering work of Wuerker et al. [2] who investigated single trapped aluminum microparticles inside a quadrupole ion trap by collecting scattered UV light. Utilization of this light scattering scheme has enabled us to obtain the mass spectra of single submicron-sized particles with the quadrupole ion trap operating in an axial mass-selective instability mode [18,19]. Extension of the work to particles with size (d) smaller than 100 nm, however, was unsuccessful. This is understood from the Rayleigh scattering theory [20], which predicts that the intensity of the scattered laser light should scale with d^{-6} for small particles. A means based upon detection of laser-induced fluorescence (LIF) has been proposed [21]. The method is conceptually simple: one can always tag nanoparticles or high-mass biomolecules of interest with dye molecules [22], making them visible to photomultipliers upon laser excitation. If the mass of the attached dye molecules is known, information about the m/z values of the original nanoparticles or biomolecules can be deduced. Since LIF is a highly sensitive method [23] and is potentially applicable to detection of any ions (large or small) that are intrinsically fluorescent or extrinsically labeled with dye molecules, the limitations as imposed on the ionization-based detectors can thereby be circumvented.

In employing LIF as the detection method, the challenge lies in how to produce and collect enough photons from them. For charged nanoparticles ejected from a quadrupole ion trap, they typically have a velocity higher than 10 m s^{-1} [18]. This suggests a laser–particle interaction time of less than 100 μs as the particle pass across a probing laser beam with a size of 1 mm. Such a time is clearly too short to produce a sufficient amount of fluorescence for detection. Deceleration of the moving particles to elongate the laser excitation time with a pair of Millikan-type plates [24] appears to be a feasible approach; however, the plates lack the ability of focusing the trap-ejected particle beam in space. In contrast, the quadrupole ion trap is ideal to serve this purpose, and the device has been proven to be capable of trapping and concentrating dye molecules in free space for optical detection over a long period of time [25,26].

We have previously demonstrated [27] that fluorescently labeled nanoparticles in a quadrupole ion trap can be generated by MALDI and detected by LIF using an Ar ion laser. With LIF, observation of the individual polystyrene particles (27 nm in diameter and fluorescently labeled with 180 fluorescein equivalents) can be achieved with an average signal-to-noise ratio (S/N) of ∼10. Additionally, to effectively confine particles with $m > 5$ MDa in space, damping of the particles' motions in the trap by employing ∼50 mTorr He buffer gas is required. Similar observations were made for particles with a nominal size of 1 μm in diameter. Both the studies pave the way to the present proposition of using laser-induced fluorescence/ion trap (LIF-IT) as a detector for ion trap mass spectrometry of nanoparticles and high-mass biomolecules [21].

2. Experiments

Details of the experimental setup have been described in [21,27], and therefore only some salient features are given here. Fig. 1 shows a schematic diagram of the dual quadrupole ion trap mass spectrometer [21], in which the first trap (T1) serves as a standard ion storage and mass analysis device, and the second trap (T2) is employed for trapping and concentrating particles ejected from T1 for LIF detection. Both traps are identical with dimensions of $r_0 = 10$ and $z_0 = 7.07$ mm. Aside from the LIF-IT detector, the spectrometer is also equipped with a channeltron (H-305A, De-Tech) to detect low-mass species for calibration purposes. The channeltron was positioned on the other side of T1 (with respect to the LIF-IT) and operated at a voltage of −2350 V. Detection efficiency was improved through the use of a deflection plate floated at −350 V.

Fluorescently labeled polystyrene particles (FluoSpheres, Molecular Probes) of sizes of 27 ± 4 and 110 ± 8 nm were used as the samples. The particles, containing 180 and 7400 fluorescein equivalents, respectively, absorb strongly at 490 nm and emit photons at 515 nm with a quantum yield of ≥30%. They were introduced into the trap by MALDI using a frequency-tripled YAG laser (5 mJ per pulse at 355 nm) through two holes on the ring electrode of T1 (cf. Fig. 1). A constant He buffer gas pressure was maintained at $P = 50$ mTorr to assist trapping the MALDI-generated charged particles. To acquire the mass spectra, the ion trap was operated in an axial mass-selective instability mode by scanning the trap driving frequency ($\Omega/2\pi$), accessible from 0.2 to 500 kHz, at a constant voltage (V_{ac}) of 200 V. Adopting this frequency scan mode avoided undesirable arcing among the three electrodes in the presence of the high-pressure buffer gas. A Labview data acquisition system controlled the frequency scan via a functional generator (DS345, Standard Research) and a home-made wide band power amplifier [28].

An argon ion laser operating at 488 nm and 400–600 mW detected nanoparticles ejected from T1 and captured by T2.

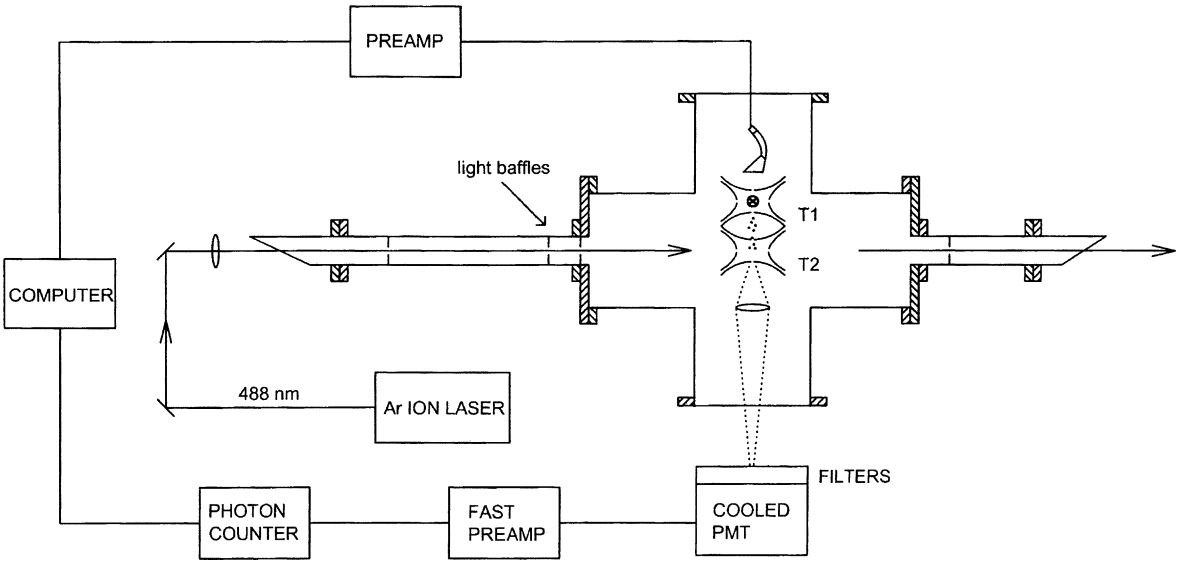

Fig. 1. Top view of a home-built dual quadrupole ion trap mass spectrometer. Two independent function generators and power amplifiers are used to drive two traps (denoted by T1 and T2, respectively) separated by a thin Teflon sheet. The nanoparticle sample is positioned near one of the ring electrode holes of the first trap to be irradiated by a frequency-tripled Nd:YAG laser ($\lambda = 355$ nm), as denoted by the enclosed cross at the center of T1. The Ar ion laser is directed into T2 through two holes on the ring electrode to yield fluorescence at 515 nm. The spectrometer is also equipped with a channeltron for detection of molecular ions.

The laser beam was focused with an $f = 1$ m lens through one of the ring-electrode holes of T2 to have a spot size of $\sim$200 μm in the trap center. Fluorescence was collected through the exit endcap hole of T2 with an F/3 lens system and sent to a thermoelectrically cooled photomultiplier tube (R943-02, Hamamatsu) for photon counting. The typical gate time was 200 ms and the dwell time was 2 ms. As shown in Fig. 2, these two times were in synchronization of the "damp" and "dump" times of particles in T2 when using LIF-IT as a nanoparticle detector. Detailed discussions of

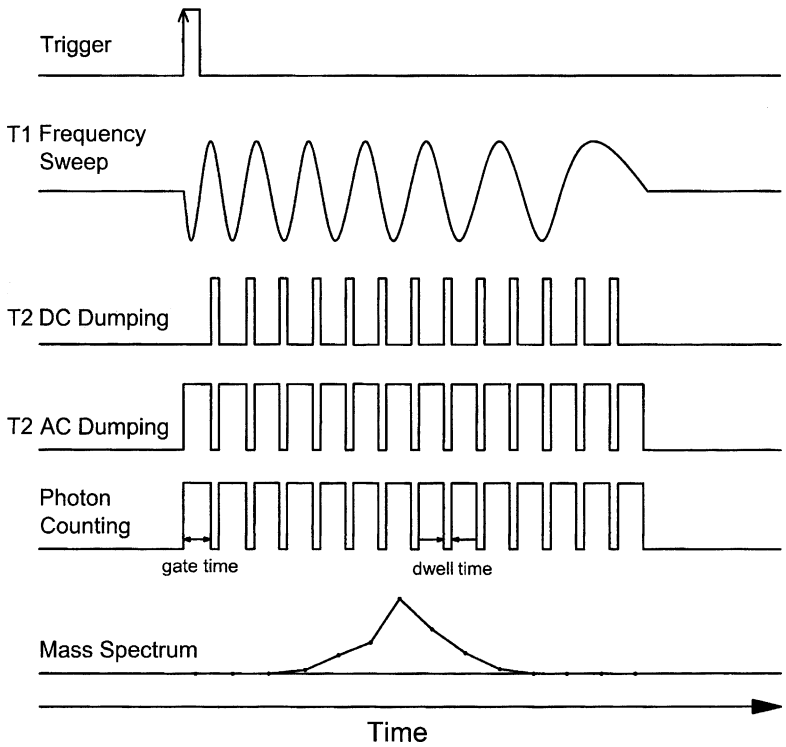

Fig. 2. Time sequences of the frequency scan, particle damping/dumping, fluorescence collection, and data acquisition used in this experiment. Note that the on–off time of the detector trap T2 is in complete synchronization with the gate-dwell time of the photon counter.

the time sequence of the trap operation and data acquisition are given in Section 3.4.

3. Results and discussion

3.1. Ion sources

MALDI and ESI are two widely used ionization methods for transporting biomolecules from condensed phases to the gas phase for m/z measurements [29]. They both are applicable to study nonvolatile organic and inorganic nanometer-sized particles as well [11,30]. While ESI is adopted more frequently in analyzing larger biomolecules because of its ability to create multiply charged ions, MALDI is advantageous in providing ions with lower charge numbers for easier interpretation of the obtained mass spectra [31]. We have tested the performance of both ion sources in our measurements [18,27], and found that MALDI is a better approach in introducing fluorescent nanoparticles into the quadrupole ion trap and in the analysis of single trapped nanoparticles by LIF in confined space.

Fig. 3a shows the result obtained with ESI and the 27 nm FluoSpheres using the detection scheme described in [27]. The fluorescence is weak and accompanied with a long decay, up to 50 s. The evidence for the existence of the charged particles in the trap is the abrupt drop of the signal when the trap power supply was turned off, as indicated by the arrow in the figure. The S/N level of the detection is poor due to the existence of the large background, which worsens after a few measurements. This is attributed to the high kinetic energy of the ESI-generated particles whose velocity (typically 300 m s^{-1}) is governed by aerodynamics rather than electrostatics [18], and most of them were not trapped but rather accumulated on the trap inner surfaces. In contrast, if MALDI was used as the ion source, a prominent signal with the excellent S/N can be obtained, as shown in Fig. 3b. The method is therefore adopted in the present measurements in transporting the fluorescent nanoparticles to the gas phase.

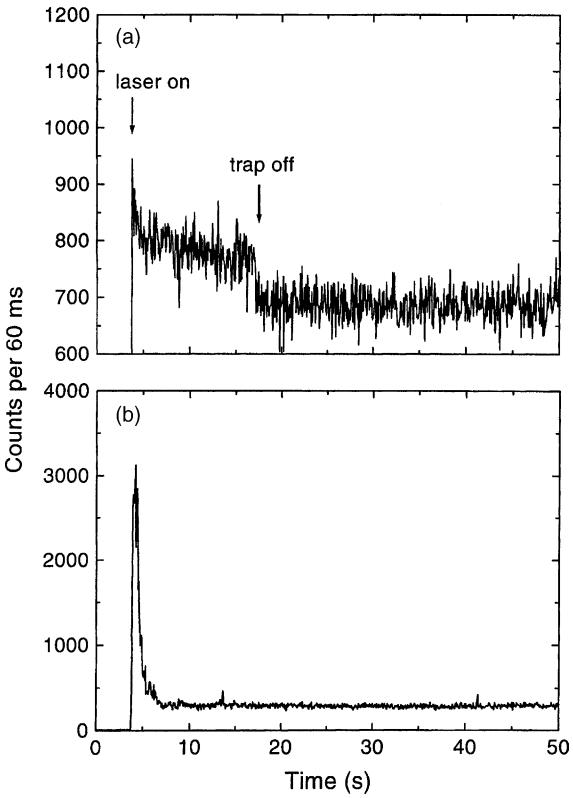

Fig. 3. (a) Time evolution of the fluorescence from trapped 27 nm particles produced by ESI. The applied dc voltage between the needle and the capillary in ESI to generate a stable spray was +4000 V [18]. The capillary (200 μm in orifice diameter and 220 mm in length) was heated to about 400 K for desolvation. A sudden drop of the signal occurred as the trap power supply was turned off (indicated by the arrow). (b) Time evolution of the fluorescence from trapped 27 nm particles generated by MALDI, as described in this experiment. The fast decay of the signal is attributed to photobleaching [27] and the trap was operated at $\Omega/2\pi = 5$ kHz and $V_{ac} = 200$ V in both measurements.

3.2. Frequency scan

Mass spectra of the polystyrene nanoparticles were acquired with the quadrupole ion trap operating in the frequency scan mode not only to avoid arcing of the electrodes in the presence of 50 mTorr He buffer gas [27] but also to widen the mass spectral analysis range [6]. According to the definition of the trap parameter [1],

$$q_z = \frac{4V_{ac}}{(m/z)r_0^2\Omega^2}, \quad (1)$$

a decrease of the trap driving frequency Ω by a factor of 10 is equivalent to increase of the trap driving voltage V_{ac} by a factor of 100. Therefore, mass spectra in a nonlinear scale would be produced as $\Omega/2\pi$ is swept down linearly. Although this is not a pleasant feature, it should not be a serious impediment, since nonlinear sweep of the frequency via proper computer softwares [32] can be implemented to obtain a linear mass spectrum.

Fig. 4 shows the mass spectra of CsI clusters and gramicidin S, obtained using the home-built ion trap mass spectrometer and the channeltron detector. The CsI clusters were produced by laser desorption/ionization of CsI crystallites with 355 nm laser pulses, while the same photons were employed to generate gramicidin S ions by MALDI with the 4-hydroxy-α-cyanocinnamic acid (4HCCA) matrix. Use of these two compounds as the reference reveals a mass uncertainty of 1% in our measurements. Compared to that of the commercial instruments [33], this uncertainty is relatively large, presumably because the applied voltage V_{ac} varies somewhat (∼1%) with $\Omega/2\pi$ over the entire frequency range of our interest (0.2–500 kHz). This uncertainty, however, should not be a matter of concern here since the nanoparticle samples used in the experiment typically have a size variation of ±10% or a mass dispersion of ±30%.

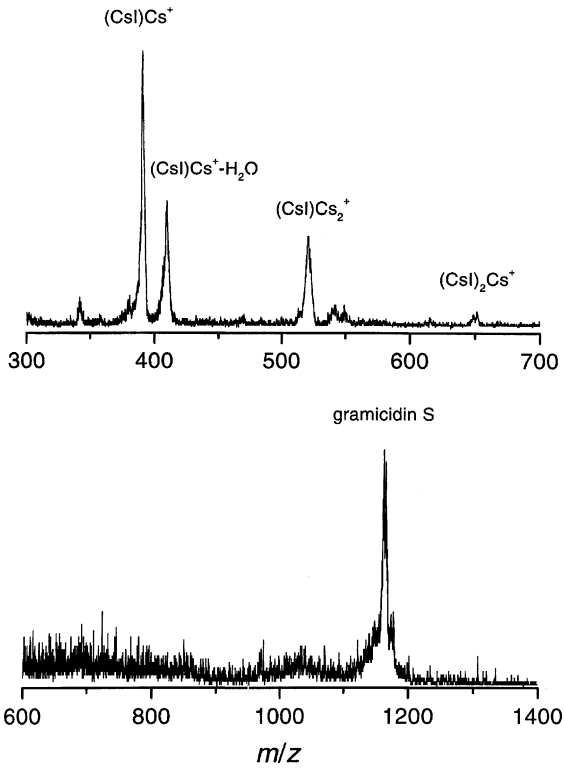

Fig. 4. Frequency scan mass spectra of CsI clusters and gramicidin S. The spectra were acquired by sweeping the trap driving frequency of T1 from 400 to 75 kHz for CsI clusters and 150 to 75 kHz for gramicidin S at a constant voltage of 200 V.

3.3. Matching of two traps

When a charged nanoparticle is transported from one quadrupole ion trap to another (T1 → T2), the q_z value of the particle follows:

$$q_{z,2} = q_{\text{eject},1}\frac{\Omega_1^2 V_{ac,2}}{\Omega_2^2 V_{ac,1}}, \quad (2)$$

where $q_{\text{eject},1}$ is the point of ion ejection from T1, $q_{z,2}$ is the corresponding value of the same ion injected into T2, Ω_1 (Ω_2) and $V_{ac,1}$ ($V_{ac,2}$) are the trap driving frequency and voltage of T1 (T2), respectively. For atomic and molecular ions, it has been well-explored [34–40] that the trapping efficiency of externally injected ions depends strongly on the q_z values of the individual entities entering the trap. Appelhans and Dahl [40] have shown specifically for Cs^+ that capture of the externally injected ions through the endcap hole of a quadrupole ion trap is effective only under limited conditions. Both simulations and measurements indicate that the ion trapping efficiency is highest at $q_z = 0.1$–0.3 over the kinetic energy range of KE = 6–24 eV [40]. It suggests that when using LIF-IT as a nanoparticle detector, selection of appropriate Ω_2 and $V_{ac,2}$ to match with the optimal $q_{z,2}$ values of the injected particles is of critical importance.

No measurements for the kinetic energies of the trap-ejected particles have been attempted in this work. Guidance for the value of KE, however, can be derived from the axial velocity of the particle at the point of ejection, namely $\omega_{z,1} = \Omega_1/2$ at $q_{z,1} = 0.908$ [41,42]. Reiser et al. [42] have shown both experimentally and numerically that the axial velocities of molecular ions ejected from the quadrupole ion trap are all similar and can be approximated by $\upsilon_0 \approx \Omega_1 z_0/2$. The approximation has also been validated in our previous measurements for the trap-ejected sub-micron-sized particles [18]. On the basis of this approximation, we estimate that any particles that are ejected from our trap at the frequency $\Omega_1/2\pi = 3$ kHz should have an initial velocity of $\upsilon_0 \approx 60\,\text{m s}^{-1}$. The velocity, however, will gradually decrease due to collisions of the particles with background gas. At the He buffer gas pressure of 50 mTorr, the trap-ejected particles are expected to reach a final velocity of $\upsilon \approx 20\,\text{m s}^{-1}$ after traveling ~20 mm [27] before they enter the second trap (cf. Fig. 1). This velocity ($\upsilon \approx 20\,\text{m s}^{-1}$) corresponds to a kinetic energy of KE ≈ 12 eV for the externally injected spheres of 27 nm in diameter ($m = 6.5$ MDa). Assuming that the behavior of the nanoparticle injection is similar to that of atomic and molecular ions, this leads us to the choice of the trap parameters $V_{ac,2} = 160$ V and $\Omega_2/2\pi = 6.0$ kHz for the 27 nm particles as the trap driving frequency is swept down from $\Omega_1/2\pi = 6.0$ to 0.5 kHz at $V_{ac,1} = 200$ V [21]. As for the 110 nm spheres, a reasonable choice of the parameters would be $V_{ac,2} = 160$ V and $\Omega_2/2\pi = 1.0$ kHz as $\Omega_1/2\pi = 1.0 \rightarrow 0.2$ kHz at $V_{ac,1} = 200$ V.

An elegant way to keep $q_{z,2}$ constant over the entire range of the mass scan is to sweep the frequency of the second trap simultaneously with the frequency of the first trap and so the condition $q_{z,2} \approx 0.1$ is always satisfied. This can be accomplished with computer programming, by which the frequency sweeps of these two traps are synchronized to maintain $\Omega_2/\Omega_1 \approx 3$ at $V_{ac,1} = V_{ac,2}$. The problematic mass discrimination associated with T2 can thereby be minimized when using LIF-IT as a nanoparticle detector.

3.4. Particle damping and dumping

One key feature of the present setup is that use of He buffer gas at a steady pressure of 50 mTorr is required to slow down the injected particles and confine them in the center of the second ion trap to be interrogated by the focused laser beam. This, however, takes time for the particle damping to complete. To obtain the LIF-based mass spectrum with good S/N in practical application, the damping time should be made as short as possible. We have inspected this quantity by recording the fluorescence signals upon rapid ejection of the particles out of T1 within 200 ms ($V_{ac,1} = 200$ V and $\Omega_1/2\pi = 6.0 \rightarrow 0.5$ kHz). Fig. 5a shows the time profile of the LIF from the 27 nm spheres, of which the fluorescence is seen to have a rise time of ~0.2 s and a decay time of ~3 s. The latter has been attributed to the photobleaching time of the fluorescein molecules under continuous Ar ion laser excitation [27].

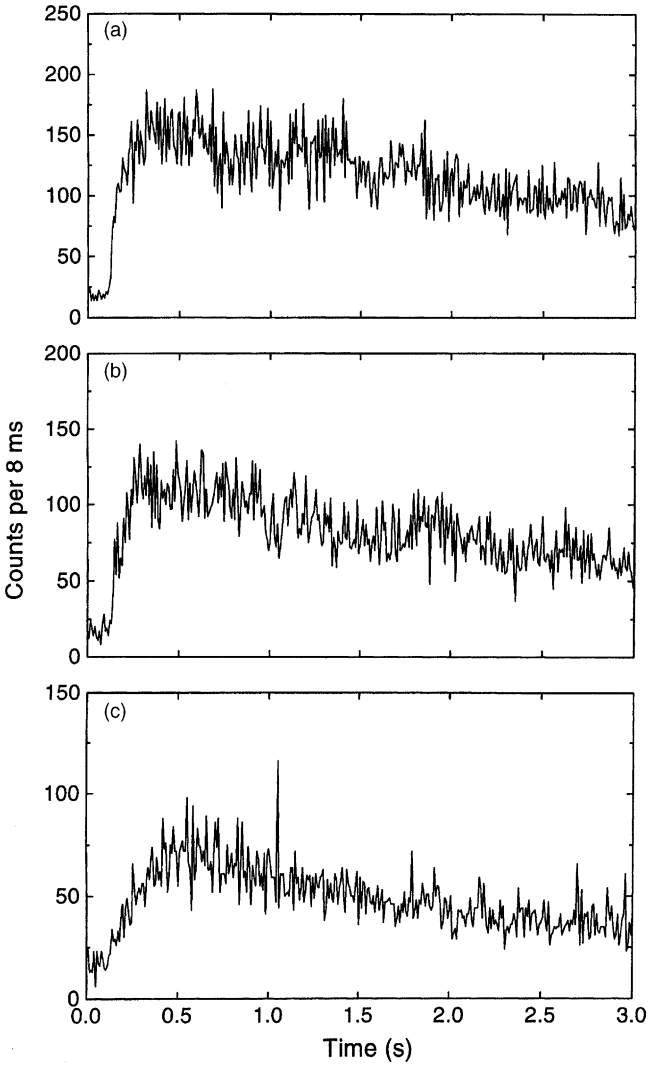

Fig. 5. Temporal profiles of the fluorescence from trapped 27 nm particles in T2 at $\Omega_2/2\pi = 6.0$ kHz and three different trap driving voltages of (a) $V_{ac,2} = 160$ V, (b) $V_{ac,2} = 100$ V, and (c) $V_{ac,2} = 60$ V. The particles were ejected out of T1 in 200 ms at a constant He buffer gas pressure of 50 mTorr. An increase in rise time of the fluorescence signal from ~0.2 to ~0.5 s is seen from (a) to (c). The power of the Ar ion laser used for the excitation was 600 mW.

The observed damping time of ~0.2 s is much longer than what we expect from molecule-particle collisions. Dahneke [43] has shown that for a sphere in thermal equilibrium with background gas molecules, the damping force can be expressed in terms of $F_d = -k_d \upsilon$ with

$$k_d = \frac{8 + \pi f}{4} \frac{pm}{\rho_0 d} \sqrt{\frac{8M}{\pi k_B T}}, \tag{3}$$

where $f \approx 0.9$ is the fraction of molecules reflected in a diffuse manner, p is the buffer gas pressure, M and T are the molar weight and temperature of the buffer gas molecules, and υ, ρ_0 and d are the velocity, density and diameter of the investigated particle, respectively. Hars and Tass [44] have further shown that damping of the motion of a charged particle in an oscillatory field (without a dc field) has a characteristic time of

$$\tau_d = \frac{2m}{k_d}. \tag{4}$$

With $d = 27$ nm, $\rho_0 = 1.05\,\mathrm{g\,cm^{-3}}$, $P = 50$ mTorr, $M = 4\,\mathrm{g\,mol^{-1}}$, and $T = 300$ K, we have $\tau_d \approx 1$ ms, which means that it will take only about 1 ms to bring one single 27 nm particle to the trap center by the 50 mTorr He buffer gas.

We attribute the discrepancy between our observation ($\tau_d \approx 200$ ms) and estimation ($\tau_d \approx 1$ ms) to the space charge effect. It is comprehensible that if damping one single charged particle takes 1 ms, a much longer time would be required for damping an ensemble of charged particles to the trap center due to the repulsions between them. In this context, decreasing the trap driving voltage should result in an increase in the damping time, since the particles are allowed to distribute over a larger volume in space and take a longer time to relax. The point is indeed verified in Fig. 5a and c, where the detected damping time is shown to increase from $\tau_d \approx 0.2$ s at $V_{ac,2} = 160$ V to $\tau_d \approx 0.5$ s at $V_{ac,2} = 60$ V. There is essentially no change in τ_d as the buffer gas pressure was varied over the range 30–80 mTorr. A gate time of 200 ms in photon counting is therefore chosen for data acquisition of the mass spectra in this experiment.

Fig. 6a displays the spectrum taken at a gate time of 200 ms and a dwell time of 2 ms with $\Omega_1/2\pi$ swept from 6.0 to 0.5 kHz for the 27 nm spheres. No m/z information is attainable due to accumulation of the fluorescent particles in T2. Clearly, the particles need to be dumped after collection of each data point. Fig. 6b shows the mass spectrum acquired with particle dumping, made possible by switching off the power supply of the detection trap for 2 ms, followed by application of a short dc pulse (2 ms and −100 V) to the exit endcap electrode of T2 in each data collection step. Sharp features derived from nanoparticles of different m/z are revealed (Fig. 6b). It is noticed that switching off the trap power supply for 2 ms alone (without the dc pulse) is insufficient to empty the trap completely. Elongation of the dumping time to 20 ms is required to eliminate the remaining background, as shown in Fig. 6c.

One may achieve a more comprehensive understanding of the particle dumping in competition with the damping from a simple analysis. Following Zerega et al. [45], we write the equation of motion for a charged particle when the trapping field is replaced by a pulsed dc field that ejects the ion toward the exit endcap as

$$m\frac{d^2z}{dt^2} = -k_d\frac{dz}{dt} + \frac{QeU}{2z_0}, \tag{5}$$

where z_0 is the distance between the endcap electrode and the trap center, U is the amplitude of the ejection dc field applied to one of the endcap electrodes, Q is the charge of

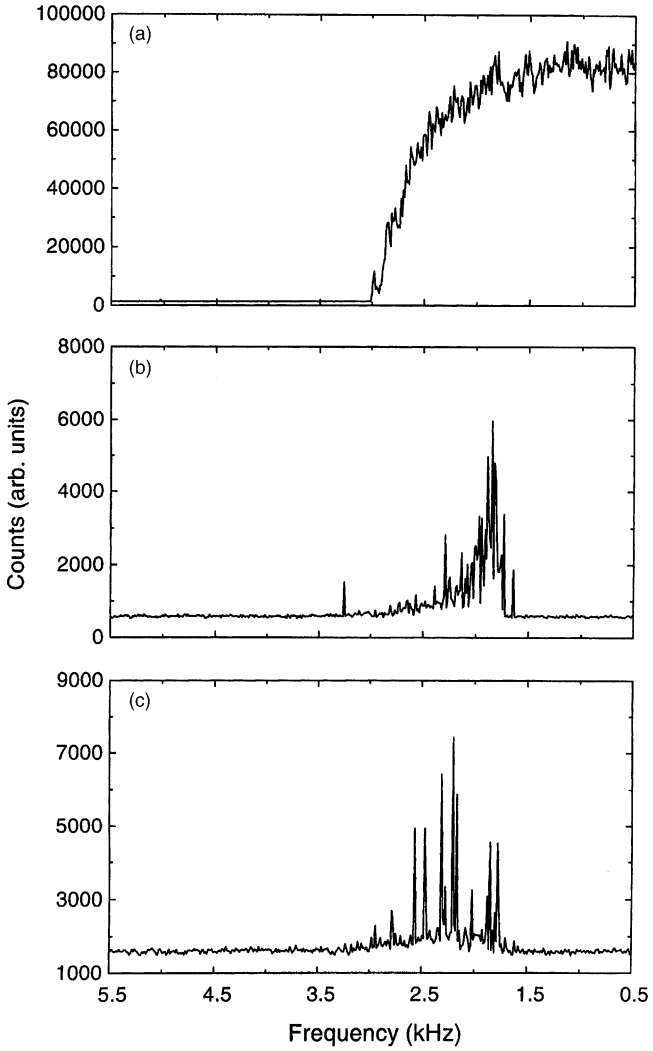

Fig. 6. Mass spectra of 27 nm fluorescent spheres, obtained by sweeping $\Omega/2\pi$ from 6.0 to 0.5 kHz under the conditions: (a) without particle dumping, (b) with particle dumping by switching off the trap power supply followed by application of a dc pulse (−100 V) to the exit endcap electrode for 2 ms, and (c) with particle dumping by switching off the trap power supply for 20 ms only. The power of the Ar ion laser used for detection was 600 mW.

the carrier, and e is the elementary charge. The distance that the particle travels with time is then

$$S(t) - S(0) = \frac{m}{k_d}\left[\frac{QeU}{2k_d z_0} - \dot{z}(0)\right](e^{-k_d t/m} - 1) + \frac{QeU}{2k_d z_0}t, \quad (6)$$

where $\dot{z}(0)$ is the initial velocity along the axial direction. Since the particles are already damped to the trap center (i.e. $S(0) \approx 0$) before the dump function is activated, they typically have an average velocity of $\sim 10\,\mathrm{m\,s^{-1}}$ under our trapping conditions [1]. Fig. 7 shows the result of the calculation for the 27 nm spheres by considering only the limiting case that the particles are initially moving opposite to the direction of the applied dc field. With $\dot{z}(0) = -10\,\mathrm{m\,s^{-1}}$,

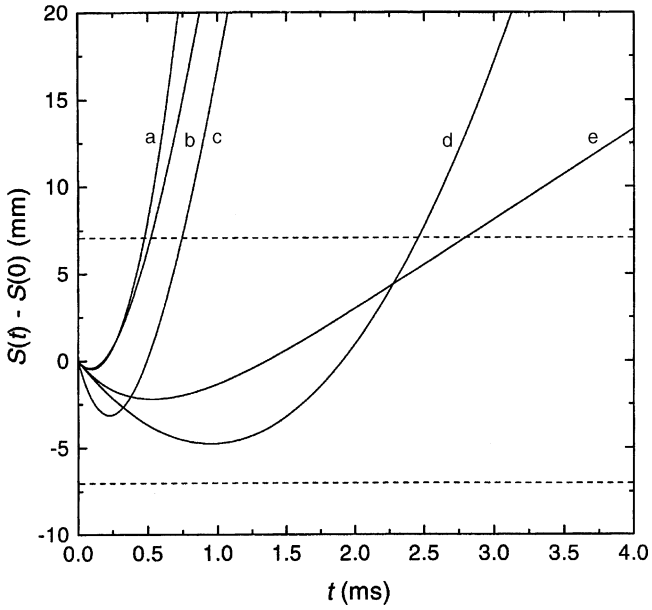

Fig. 7. Calculated dumping times of trapped 27 nm spheres in T2. The particles were dumped by switching off the trap power supply followed by application of a pulsed dc voltage to the exit endcap electrode. The parameters used in the computation are: (a) $U = 100\,\mathrm{V}$, $\dot{z}(0) = -10\,\mathrm{m\,s^{-1}}$, $k_d/m = 0\,\mathrm{s^{-1}}$; (b) $U = 100\,\mathrm{V}$, $\dot{z}(0) = -10\,\mathrm{m\,s^{-1}}$, $k_d/m = 2000\,\mathrm{s^{-1}}$; (c) $U = 100\,\mathrm{V}$, $\dot{z}(0) = -30\,\mathrm{m\,s^{-1}}$, $k_d/m = 2000\,\mathrm{s^{-1}}$; (d) $U = 10\,\mathrm{V}$, $\dot{z}(0) = -10\,\mathrm{m\,s^{-1}}$, $k_d/m = 0\,\mathrm{s^{-1}}$; and (e) $U = 10\,\mathrm{V}$, $\dot{z}(0) = -10\,\mathrm{m\,s^{-1}}$, $k_d/m = 2000\,\mathrm{s^{-1}}$. The dash lines denote the points of particle ejection at $z = \pm 7.07$ mm.

$Q = +1$, $U = 10\,\mathrm{V}$, and $P = 50\,\mathrm{mTorr}$, a time of $t_d \approx 3\,\mathrm{ms}$ is calculated for the particle to reach the exit endcap ($S(t_d) - S(0) = 7.07\,\mathrm{mm}$). Increasing the voltage to $U = 100\,\mathrm{V}$, however, can effectively reduce the dumping time to $t_d < 1\,\mathrm{ms}$, even with $\dot{z}(0) = -30\,\mathrm{m\,s^{-1}}$ as shown in the figure. It indicates that the t_d is not a strong function of $\dot{z}(0)$ when high dc voltages are applied. In Fig. 7, we also compare the calculated results with and without buffer gas at $U = 10$ and 100 V. The influence of the 50 mTorr He buffer gas on the dumping time is seen to diminish almost completely at $U = 100\,\mathrm{V}$, where all the particles are ejected out of the exit endcap within 1 ms. Our choice of 2 ms dumping time and 100 V pulsed dc field thus suffices to solve the particle accumulation problem, particularly for multiply charged species.

3.5. Detection limits

Displayed in Fig. 8a is a single-scan mass spectrum of the 27 nm spheres, each of which has a mean molecular mass of 6.5 MDa. Irregular features are seen to spread over a wide m/z range from 2×10^6 to 9×10^6. A smoother spectral profile emerges after accumulation of 10 single-scan mass spectra (Fig. 8b). The majority of the features are centered on $m/z \approx 6.5 \times 10^6$, suggesting that the spectrum is predominantly contributed from singly charged particles. Although there is a lack of proper mass calibrants in this m/z region,

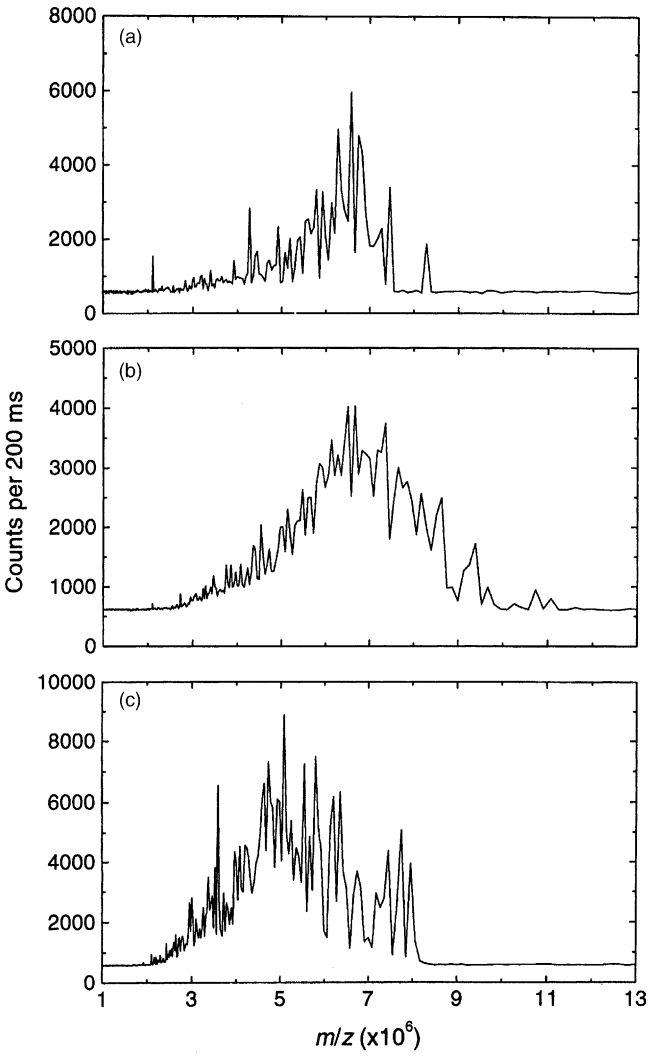

Fig. 8. Mass spectra of 27 nm fluorescent spheres, obtained from (a) 1 scan and (b, c) averaging of 10 scans. All the spectra were acquired by sweeping $\Omega_1/2\pi$ from 6.0 to 0.5 kHz at $V_{ac,1} = 200$ V under the conditions: (a, b) $\Omega_2/2\pi = 6.0$ kHz at $V_{ac,2} = 160$ V and (c) sweeping of $\Omega_2/2\pi$ from 18 to 1.5 kHz at $V_{ac,2} = 160$ V (see text for detail). The power of the Ar ion laser used for detection was 600 mW.

we calibrate the mass spectra using the point of ejection, $q_{eject,1} \approx 0.95$ (rather than 0.908), as determined in our previous experiments for 1 μm particles [19].

In Fig. 8, we also compare the spectrum (b) acquired with the trap driving frequency fixed at $\Omega_2/2\pi = 6.0$ kHz and the spectrum (c) acquired with the frequency $\Omega_2/2\pi$ scanned along with $\Omega_1/2\pi = 6.0 \rightarrow 0.5$ kHz to maintain $q_{z,2} \approx 0.1$, as discussed in the earlier section. The spectrum is seen to shift to the lower m/z region as the way of data collection is changed from (b) to (c). Clearly, there are more doubly charged particles captured by T2 under the dynamic trapping condition (c) than the static trapping condition (b). The result is in line with our previous observation [21], where the maximum of the spectrum shifted from $m/z \approx 5.5 \times 10^6$ to 3.1×10^6 when $V_{ac,2}$ was lowered from 160 to 60 V.

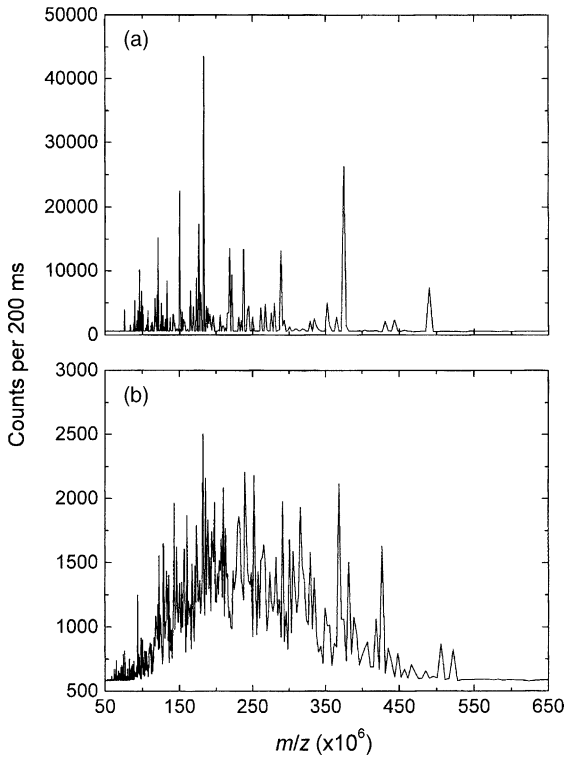

Fig. 9. Mass spectra of 110 nm fluorescent spheres, obtained from (a) 1 scan and (b) averaging of 100 scans. The spectra were acquired by sweeping $\Omega_1/2\pi$ from 1.0 to 0.2 kHz at $V_{ac,1} = 200$ V, $\Omega_2/2\pi = 1.0$ kHz, and $V_{ac,2} = 160$ V. The power of the Ar ion laser used for detection was 400 mW.

In addition to the detection of the 27 nm spheres, the LIF-IT is capable of detecting 110 nm particles as well. Fig. 9a shows the single-scan mass spectrum acquired by sweeping down the frequency from $\Omega_1/2\pi = 1.0$ to 0.2 kHz at $V_{ac,1} = 200$ V, which covers the m/z range of 48×10^6–1200×10^6. For the 110 nm fluorescent spheres, they have a mean mass of 440 MDa, but with a mass distribution of 350–543 MDa due to the size variation of ±8 nm. This suggests a m/z range of (350–543) $\times 10^6$ to (58–91) $\times 10^6$ for particles carrying 1–6 charges. Similar to the result of the 27 nm spheres, all the features derived from multiply charged particles can be identified in the statistically averaged spectrum (Fig. 9b). Comparison of the spectra displayed in Figs. 8 and 9 indicates that roughly twice amount of the charges is being carried by the larger particles.

We estimate that for particles generated by MALDI and trapped in T1, roughly 10% of them will enter T2 upon the mass-selective axial ejection. This is because (1) equal portions of the particles are being ejected from the two endcap electrodes of T1, (2) some of the ejected particles are lost during the particle transport from T1 to T2, and (3) part of the ejected particles cannot be captured by T2 because of the phase mismatching problem in particle injection [6,34]. Therefore, if there are 10^3 charged particles in T1 to begin with, only 10^2 of them would be detected by LIF in T2 over

the entire range of frequency scan. Since the nanoparticles used in this experiment all differ somewhat in mass and charge number from each other not surprisingly, such a low particle density would give rise to well-separated peaks as observed experimentally (cf. Fig. 9a).

It is likely that the sharp and well-separated features observed in Fig. 9a are derived from the individual 110 nm FluoSpheres. The likelihood is high because each one of them contains 7400 fluorescein equivalents and should be easily detected. Despite there is a lack of direct evidence at this moment to corroborate the suggestion that the individual spectral features are indeed derived from single particles, the excellent S/N of the spectrum indicates that particles that are fluorescently labeled with 10 fluorescein molecules or less can be detected with the LIF-IT technique [21]. Since the dye labeling is, in principle, applicable to particles of any size, the spectral analysis range of the ion trap mass spectrometer equipped with the LIF-IT is essentially limitless.

3.6. Practical considerations

The detection sensitivity of the present setup may be enhanced 10-fold by increasing the light collection efficiency using optics with an F/1 lens system [46]. To enhance the sensitivity further, a more open trapping device [47,48] can be implemented to minimize the level of the background scattered laser light. With these improvements, a blue diode laser or a high-power LED ($\lambda = 473$ nm) may substitute the Ar ion laser as the light source to reduce the cost of using LIF-IT as a nanoparticle detector [49]. Furthermore, by employing the sample-specific dye-labeling technique [22], differentiation of nanoparticles of different origins is possible through multicolor fluorescence spectroscopy [50] with the aid of laser diodes. This, in effect, would add a new dimension to mass spectral analysis of nanoparticles.

The presently developed technique is expected to find useful applications in mass analysis of biologically important particles, such as viruses and other biomolecular assemblies [51,52]. The application appears to be practical since dye labeling has been a routine protocol in life science research. Although the LIF technique is inconvenient in that one needs to quantify the extent of dye labeling prior to the mass spectrometric analysis, the disadvantage can be readily overcome by optical detection of the amount of dye molecules attached to the bioparticles [22]. Compared to the ESI-TOF mass spectrometry performed on large biomolecular species by Robinson and coworkers [51], the MALDI–LIF-ITMS clearly offers the advantage that it does not require the particles to carry multiple charges for detection, a requirement which often makes spectral assignment indirect and difficult. We have demonstrated the utility of this new mass spectrometric method in biological macromolecular analysis with fluorescently labeled IgG ($m \approx 150$ kDa) [21].

4. Conclusion

We have developed a novel method to obtain the mass spectra of intrinsically fluorescent or fluorescently labeled nanoparticles with sizes in the range of 10–100 nm. In contrast to the conventional ion trap mass spectrometer, typically equipped with an electron multiplier, this new type of mass spectrometer is equipped with a continuous-wave laser, a photomultiplier tube, and a second ion trap for particle detection. It is an optical approach and, in principle, has no size limitations and is applicable to detection of any particles once they are fluorescently labeled. We have demonstrated the utilities of this new mass spectrometer using fluorescently labeled polystyrene nanoparticles of sizes of 27 and 110 nm as the examples. Further improvement of the performance (both in mass measurement accuracy and in detection sensitivity) of the prototypic mass spectrometer is expected to bring the instrument to a stage of practical applications, not only in life science research but also in nanosciences and nanotechnologies.

Acknowledgements

We acknowledge the Academia Sinica and the National Science Council (Grant No. NSC 91-3112-P-001-023-Y) of Taiwan for financial support of this work.

References

[1] R.E. March, R.J. Hughes, Quadrupole Storage Mass Spectrometer, Wiley, New York, 1989.
[2] R.F. Wuerker, H. Shelton, R.V. Langmuir, J. Appl. Phys. 30 (1959) 342.
[3] R.E. March, J.F.J. Todd (Eds.), Practical Aspects of Ion Trap Mass Spectrometry, vol. 1, CRC Press, Boca Raton, FL, 1995.
[4] I.S. Gilmore, M.P. Seah, Int. J. Mass Spectrom. 202 (2000) 217.
[5] R.E. March, Int. J. Mass Spectrom. 200 (2000) 285.
[6] U.P. Schlunegger, M. Stoeckli, R.M. Caprioli, Rapid Commun. Mass Spectrom. 13 (1999) 1792.
[7] S. Berkenkamp, F. Kirpekar, F. Hillenkamp, Science 281 (1998) 260.
[8] M.A. Park, J.H. Callahan, Rapid Commun. Mass Spectrom. 8 (1994) 317.
[9] D.C. Imrie, J.M. Pentney, J.S. Cottrell, Rapid Commun. Mass Spectrom. 9 (1995) 1293.
[10] U. Bahr, U. Röhling, C. Lautz, K. Strupat, M. Schürenberg, F. Hillenkamp, Int. J. Mass Spectrom. Ion Process. 153 (1996) 9.
[11] S.D. Fuerstenau, W.H. Benner, Rapid Commun. Mass Spectrom. 9 (1995) 1528.
[12] W.H. Benner, Anal. Chem. 69 (1997) 4162.
[13] J.C. Schultz, C.A. Hack, W.H. Benner, J. Am. Soc. Mass Spectrom. 9 (1998) 305.
[14] D. Twerenbold, Nucl. Instr. Meth. A 370 (1996) 253.
[15] G.C. Hilton, J.M. Martinis, D.A. Wollman, K.D. Irwin, L.L. Dulcie, D. Gerber, P.M. Gillevet, D. Twerenbold, Nature 391 (1998) 672.
[16] M. Frank, S.E. Labov, G. Westmacott, W.H. Benner, Mass Spectrom. Rev. 18 (1999) 155.
[17] M. Frank, Nucl. Instr. Meth. A 444 (2000) 375.
[18] Y. Cai, W.-P. Peng, S.-J. Kuo, Y.T. Lee, H.-C. Chang, Anal. Chem. 74 (2002) 232.

[19] Y. Cai, W.-P. Peng, S.-J. Kuo, H.-C. Chang, Int. J. Mass Spectrom. 214 (2002) 63.
[20] H.C. Van de Hulst, Light Scattering by Small Particles, Wiley, New York, 1957.
[21] Y. Cai, W.-P. Peng, H.-C. Chang, Anal. Chem. 75 (2003) 1805.
[22] R.P. Haugland, Handbook of Fluorescent Probes and Research Chemicals, 6th ed., Molecular Probes, Eugene, 1996.
[23] X.S. Xie, J.K. Trautman, Annu. Rev. Phys. Chem. 49 (1998) 441.
[24] E.J. Davis, Aerosol Sci. Tech. 26 (1997) 212.
[25] W.B. Whitten, J.M. Ramsey, S. Arnold, B.V. Bronk, Anal. Chem. 63 (1991) 1027.
[26] J.T. Khoury, S.E. Rodriguez-Cruz, J.H. Parks, J. Am. Soc. Mass Spectrom. 13 (2002) 696.
[27] Y. Cai, W.-P. Peng, S.-J. Kuo, C.-C. Han, S. Sabu, H.-C. Chang, Anal. Chem. 74 (2002) 4434.
[28] J. Ting, EDN 46 (2001) 136.
[29] C. Dass, Principles and Practices of Biological Mass Spectrometry, Wiley, New York, 2001.
[30] D.C. Schriemer, L. Li, Anal. Chem. 68 (1996) 2721.
[31] M. Scalf, M.S. Westphall, J. Krause, S.L. Kaufman, L.M. Smith, Science 283 (1999) 194.
[32] L. Ding, M. Sudakov, S. Kumashiro, Int. J. Mass Spectrom. 221 (2002) 117.
[33] J. Qin, R.J.J.M. Steenvoorden, B.T. Chait, Anal. Chem. 68 (1996) 1784.
[34] C. Weil, M. Nappi, C.D. Cleven, H. Wollnik, R.G. Cooks, Rapid Commun. Mass Spectrom. 10 (1996) 742.
[35] V.M. Doroshenko, R.J. Cotter, J. Mass Spectrom. 31 (1997) 602.
[36] L. He, D.M. Lubman, Rapid Commun. Mass Spectrom. 11 (1997) 1467.
[37] S.T. Quarmby, R.A. Yost, Int. J. Mass Spectrom. 190/191 (1999) 81.
[38] V. Steiner, C. Beaugrand, P. Liere, J.-C. Tabet, J. Mass Spectrom. 34 (1999) 511.
[39] K. Yoshinari, Rapid Commun. Mass Spectrom. 14 (2000) 215.
[40] A.D. Appelhans, D.A. Dahl, Int. J. Mass Spectrom. 216 (2002) 269.
[41] C. Marinach, A. Brunot, C. Beaugrand, G.G. Bolbach, J.C. Tabet, Int. J. Mass Spectrom. 213 (2002) 45.
[42] H.-P. Reiser, R.E. Kaiser, P.J. Savickas, R.G. Cooks, Int. J. Mass Spectrom. Ion Process. 106 (1991) 237.
[43] B.E. Dahneke, Aerosol Sci. 4 (1973) 147.
[44] G. Hars, Z. Tass, J. Appl. Phys. 77 (1995) 4245.
[45] Y. Zerega, P. Perrier, M. Carette, G. Brincourt, T. Nguema, J. Andre, Int. J. Mass Spectrom. 190/191 (1999) 59.
[46] M.D. Barnes, K.C. Ng, W.B. Whitten, J.M. Ramsey, Anal. Chem. 65 (1993) 2360.
[47] S. Schlemmer, J. Illemann, S. Wellert, D. Gerlich, J. Appl. Phys. 90 (2001) 5410.
[48] S. Arnold, N.L. Goddard, N. Wotherspoon, Rev. Sci. Instrum. 70 (1999) 1473.
[49] S.-C. Wang, M.D. Morris, Anal. Chem. 72 (2000) 1448.
[50] J.R. Taylor, M.M. Fang, S. Nie, Anal. Chem. 72 (2000) 1979.
[51] M.A. Tito, K. Tars, K. Valegard, J. Hajdu, C.V. Robinson, J. Am. Chem. Soc. 122 (2000) 3550;
A.A. Rostom, P. Fucini, D.R. Benjamin, R. Juenemann, K.H. Nierhaus, F.U. Hartl, C.M. Dobson, C.V. Robinson, Proc. Natl. Acad. Sci. U.S.A. 97 (2000) 5185.
[52] S.D. Fuerstenau, W.H. Benner, J.J. Thomas, C. Brugidou, B. Bothner, G. Siuzdak, Angew. Chem. Int. Ed. 40 (2001) 541.